Frontiers in Computing and Intelligent Systems
ISSN: 2832-6024 | Vol. 15, No. 3, 2026

Research on Downhole Low-Frequency Electromagnetic Wave Wireless Transmission based on Differential Phase Shift Keying and Forward Error Correction Codes

Jiarui Cheng [1, *], Zhiao Du [1], Zewei Pan [2], Jinlong Wang [2], Wenlan Wei [1]

[1] School of Mechanical Engineering, Xi'an Shiyou University, Xi'an, Shaanxi 710065, China
[2] China Oilfield Services Limited Integrated Solution & New Energy Division, Tianjin 300459, China

*** Corresponding author:** Jiarui Cheng

Abstract: Due to the complex downhole environment in oil and gas wells, electromagnetic wave wireless transmission suffers from high attenuation, multipath interference, and low signal-to-noise ratio, making long-distance and reliable communication difficult. To address these challenges, a composite modulation method combining Differential Phase Shift Keying (DPSK) and Forward Error Correction (FEC) is proposed. A downhole channel model incorporating path loss, multipath effects, and noise interference was established, and a transmitting–receiving hardware system was designed. Signal transmission characteristics in different media were experimentally investigated to analyze electromagnetic signal propagation behavior. The encoding and decoding performance of the DPSK–FEC scheme was evaluated through MATLAB simulations, focusing on the phase disturbance resistance of DPSK and the error correction capability of FEC. The coding parameters were further optimized to match downhole channel characteristics. The non-coherent demodulation mechanism of DPSK provides robustness against phase noise and frequency drift, while FEC introduces redundancy to detect and correct transmission errors, significantly improving system reliability. Experimental results show that the proposed system can operate stably at a depth of 1000 m and an environmental temperature of 75°C, enabling reliable bidirectional transmission of downhole data over long distances.

Keywords: Differential Phase Shift Keying (DPSK); Forward Error Correction Coding (FEC); Electromagnetic Wave Transmission; MATLAB Simulation.

1. Introduction

As oil and gas exploration and development extend to deeper, unconventional, and complex formations [1], the demand for real-time data transmission in downhole environments is becoming increasingly urgent [2]. During the testing, exploration, and extraction operations of oil wells, it is essential to obtain real-time key information such as temperature, pressure, and location of the downhole environment [3]. Traditional downhole wired communication technologies face issues such as high deployment costs, limited channel capacity, and weak anti-interference capabilities[4], making it difficult to meet the high-reliability communication requirements under complex geological conditions.In non-continuous, gas-phase dominated conditions such as gas injection, fracturing, and gas production, acoustic wave transmission and mud pulse transmission are hindered by the discontinuity of the medium, leading to ineffective signal transmission [5]. Electromagnetic wave wireless transmission, with its strong resistance to gas interference, has become a core technological direction for information acquisition in unconventional oil and gas development scenarios.

Downhole wireless communication systems primarily rely on mud pulse transmission. This technique encodes information by generating pressure pulses through variations in mud flow rate and requires a continuous and homogeneous liquid medium as the signal carrier. However, under conditions such as gas injection wells, hydraulic fracturing, and gas production, the discontinuity of the wellbore medium and the presence of gas-dominated flow may cause mud pulse transmission to become ineffective.Acoustic communication relies on the propagation of elastic vibrations within the medium to transmit energy and information, making it highly dependent on the continuity, homogeneity, and phase composition of the medium. The propagation efficiency of acoustic waves is therefore closely related to the acoustic impedance and continuity of the medium. When phase interfaces (gas–liquid, gas–solid, or liquid–solid) exist within the medium, acoustic waves undergo reflection, refraction, and scattering at these interfaces. As a result, rapid energy attenuation occurs, preventing the effective transmission of data.

Due to their strong penetration capability in non-ideal media[6] and relatively low path loss, low-frequency electromagnetic waves (typically in the frequency range of 1 kHz–1 MHz) are considered a key technological approach for addressing the bottleneck of wireless communication in enclosed environments such as deep wells and tunnels[7]. However, in downhole environments, significant multipath effects and complex noise interference[8] often lead to limited interference resistance and low communication efficiency, which remain the primary challenges for low-frequency electromagnetic wave communication systems[9].To improve interference resistance and transmission performance, existing studies have adopted various techniques, including adaptive modulation[10], channel coding optimization[11], and multipath suppression methods[12]. For example, an adaptive bandwidth allocation strategy for low-frequency signals based on orthogonal frequency division multiplexing (OFDM) suppresses multipath interference by dynamically adjusting the subcarrier spacing[13]. In addition, some researchers have employed deep reinforcement learning to optimize the iterative decoding algorithm of low-density

parity-check (LDPC) codes, thereby improving coding gain under low signal-to-noise ratio conditions[14]. The EU "DEEP-COMS" project utilizes the low-complexity decoding characteristics of Polar codes to adapt to non-stationary downhole channels[15]. Furthermore, a research team at MIT developed a multipath channel estimation method based on compressed sensing, which combines sparse signal processing techniques to reduce noise interference[16].Nevertheless, existing technologies still face significant challenges in balancing coding redundancy and transmission efficiency under low-frequency narrowband resource constraints. In addition, the time-varying characteristics of electromagnetic noise may lead to fluctuations in decoding performance, further limiting system reliability[17].

Differential Phase Shift Keying (DPSK) is a non-coherent digital modulation technique that transmits information through phase differences between adjacent symbols[18]. By eliminating the need for carrier phase synchronization, DPSK effectively avoids the influence of carrier synchronization errors on demodulation performance, making it particularly suitable for low-frequency channels with significant multipath effects[19].However, during downhole transmission, electromagnetic signals are highly susceptible to interference caused by formation absorption, electromechanical equipment noise, and random reflections, which may lead to a significant increase in the bit error rate (BER). Under such conditions, optimization of modulation techniques alone is insufficient to satisfy the high-reliability requirements of downhole communication systems. Therefore, the integration of Forward Error Correction (FEC) technology, which introduces redundant information to detect and correct transmission errors, has become an effective approach to improving system robustness[20]. Furthermore, the combination of DPSK and FEC can enhance spectral efficiency to a certain extent, enabling low-frequency electromagnetic wave communication systems to achieve reliable and efficient data transmission even under limited spectral resources[20].

This study integrates Differential Phase Shift Keying (DPSK) with Forward Error Correction (FEC) to develop a new downhole channel model. A novel electromagnetic transmission hardware system is designed, and transmission experiments are conducted in various media to evaluate signal propagation characteristics. In addition, a downhole long-distance additive white Gaussian noise (AWGN) environment is constructed for system simulation. Signal transmission parameters are configured, and the received signal waveforms are obtained for performance analysis.

2. DPSK + FEC Modulated Electromagnetic Wave Wireless Transmission Model

2.1. Downhole Electromagnetic Wave Transmission Attenuation Model

In oil and gas wells, the downhole environment typically consists of closed or semi-closed structures such as circular wellbores and tunnels. Electromagnetic waves propagate along the wellbore in a waveguide-like mode, governed by the principles of electromagnetic induction and wave propagation described by Maxwell's equations. To simplify the analysis, it is assumed that no free charges or conduction currents exist within the wellbore, and therefore the region can be considered source-free. Based on circular waveguide theory and the fundamental laws of electromagnetic fields, Maxwell's equations can be expressed in cylindrical coordinates, as shown in Equation (1).

$$\begin{cases} \nabla \cdot \mathbf{E} = 0 \\ \nabla \cdot \mathbf{B} = 0 \\ \nabla \times \mathbf{E} = -\dfrac{\delta \mathbf{B}}{\delta t} = -j\omega\mu\mathbf{H} \\ \nabla \times \mathbf{H} = \dfrac{\delta \mathbf{D}}{\delta t} = j\omega\varepsilon\mathbf{E} \end{cases} \tag{1}$$

Where ∇ denotes the Hamiltonian operator (m^{-1}); H is the magnetic field intensity (A/m); D is the electric flux density (C/m^2); E is the electric field intensity (V/m); ε is the permittivity (F/m); and μ is the permeability (H/m).

In the downhole working environment, long-term operation and long-distance information transmission must be ensured. Under axisymmetric coordinates, Maxwell's equations can be simplified to the TE mode (in which the magnetic field has only the φ component, while the electric field has r and z components). The core iterative equations after FDTD discretization are shown in Equations (2) and (3).

$$H_{\phi}^{n+\frac{1}{2}}(i,j) = H_{\phi}^{n+\frac{1}{2}}(i,j) + \frac{\Delta t}{\mu_0}\left(\frac{E_z^n(i,j) - E_z^n(i-1,j)}{\Delta r} - \frac{E_z^n(i,j) - E_z^n(i,j-1)}{\Delta z} \right) \tag{2}$$

$$E_r^n(i,j) = \frac{1 - \dfrac{\sigma_r \Delta t}{2\varepsilon_0\varepsilon_r}}{1 + \dfrac{\sigma_r \Delta t}{2\varepsilon_0\varepsilon_r}} E_r^{n-1}(i,j) + \frac{\Delta t}{\varepsilon_0\varepsilon_r\left(1 + \dfrac{\sigma_r \Delta t}{2\varepsilon_0\varepsilon_r}\right)} \left(\frac{H_{\phi}^{n-\frac{1}{2}}(i,j) - H_{\phi}^{n-\frac{1}{2}}(i,j-1)}{\Delta z} \right) \tag{3}$$

$$E_z^n(i,j) = \frac{1 - \dfrac{\sigma_r \Delta t}{2\varepsilon_0\varepsilon_r}}{1 + \dfrac{\sigma_r \Delta t}{2\varepsilon_0\varepsilon_r}} E_z^{n-1}(i,j) - \frac{\Delta t}{\varepsilon_0\varepsilon_r\left(1 + \dfrac{\sigma_r \Delta t}{2\varepsilon_0\varepsilon_r}\right)} \left(\frac{H_{\phi}^{n-\frac{1}{2}}(i,j) - H_{\phi}^{n-\frac{1}{2}}(i-1,j)}{\Delta r} \right) \tag{4}$$

Where ε_r is the relative permittivity of the medium (F/m); ε_0 is the permittivity of free space(F/m); μ_0 is the

permeability of free space (H/m);△r, △z, and △t represent the spatial grid steps and the time step, which must satisfy the CFL stability condition.

In an axisymmetric space, the TE mode (dominated by Hφ, with coupling between E_r and E_z^n) can more accurately characterize the electromagnetic propagation characteristics of circular downhole wellbores compared with other modes. The TE mode has no lower cutoff frequency under axisymmetric constraints, making it more suitable for low-frequency, long-distance signal transmission in downhole environments.When the downhole temperature, pressure, and transmission distance are assumed to remain constant, the primary factors affecting electromagnetic wave propagation include multipath effects, noise interference, and metal shielding.Multipath effects arise from strong reflections, refractions, and scattering of electromagnetic waves caused by the wellbore inner wall, downhole equipment, and surrounding geological formations. Consequently, signals transmitted from the transmitter do not propagate along a single path but reach the receiver through multiple propagation paths. Due to differences in propagation delay and phase, these multipath components may combine constructively or destructively, resulting in signal distortion and intersymbol interference (ISI).

$$r(t) = \sum_{i=0}^{L-1} \alpha_i(t) s(t - \tau_i(t)) e^{j\phi_i(t)} + n(t) \tag{5}$$

$$\mathrm{r(t)} = \alpha_0 s(t-\tau_0) e^{j\phi_0} + a_1 s(t-\tau_1) e^{j\phi_0} + \ldots + n(t) \tag{6}$$

Equation (5) represents the impulse response of the multipath channel in the time domain, while Equation (6) describes the downhole multipath model. Where: r(t) is the time-domain signal at the receiver; L is the number of multipath components; $\alpha_i(t)$ is the time-varying attenuation factor of the i-th path; s(t) is the original signal transmitted by the transmitter; τ_i is the time-varying propagation delay of the i-th path; $\phi_i(t)$ is the time-varying phase shift of the i-th path; and n(t) is the superimposed noise signal.

Noise interference mainly includes natural noise and man-made noise. These noise sources exhibit characteristics such as wide bandwidth, non-stationarity, and strong coupling. They further superimpose on the transmitted signal, reducing the signal-to-noise ratio and increasing transmission bit errors. The receiver captures the propagated electromagnetic wave signal through an antenna and recovers the original baseband information through the demodulation process, thereby enabling wireless information transmission.

$$n(t) = n_{AWGN}(t) + n_{\mathrm{Im}p}(t) + n_{EMI}(t) + \varepsilon(t) \tag{7}$$

$$n_{AWGN}(t) \sim N(0, \sigma^2{}_{AWGN})$$

$$n_{\mathrm{Im}p}(t) = \sum_{k=0}^{K-1} A_k \delta(t - t_k) \tag{8}$$

$$n_{EMI}(t) = \sqrt{P_{EMI}} \cdot g(t) \cdot \cos(2\pi f_{EMI} t + \theta_{EMI})$$

Where: n(t) is the total downhole noise (V); n_{AWGN} is the Gaussian white noise (V); n_{Imp} is the impulsive noise (V); n_{EMI} is the electromagnetic interference noise (V); $\varepsilon(t)$ is other random noise (V); N(0,$\sigma^2{}_{AWGN}$) is the noise spectral power (W); K is the number of pulses within the observation time; A_k is the amplitude of the k-th pulse (following a Gaussian distribution); P_{EMI} is the average power of electromagnetic interference (W); g(t) is the time-varying amplitude factor (dimensionless); and f_{EMI} is the center frequency of the interference signal (Hz).

The influence of metallic shielding on electromagnetic wave transmission is mainly manifested in three aspects: reflection, absorption, and multiple reflections. When an electromagnetic wave is incident from air (or an insulating medium) onto a metal surface, the high electrical conductivity of the metal results in an intrinsic wave impedance much lower than that of air. Consequently, most of the incident electromagnetic energy is reflected at the metal surface. The portion of the electromagnetic wave that penetrates the metal induces strong eddy currents, which convert electromagnetic energy into heat and dissipate it within the material. As electromagnetic waves propagate within the metal, their amplitude attenuates exponentially, and the attenuation rate is primarily determined by the skin depth. The smaller the skin depth, the greater the absorption loss.

$$\begin{aligned} R_{pw} &= 168 - 10\log_{10}\left(\frac{f\mu_r}{\sigma_r}\right) \\ \delta &= \sqrt{\frac{2}{\omega\mu\sigma}} = \frac{1}{\sqrt{\pi f\mu\sigma}} \\ A &= 1.314 \cdot d \cdot \sqrt{f\mu_r\sigma_r} \end{aligned} \tag{9}$$

Where: δ is the skin depth (m); μ is the permeability (H/m); σ is the electrical conductivity (S/m); d is the thickness of the shielding material (cm); R is the reflection loss (dB); A is the absorption loss (dB).

Based on Maxwell's equations and circular waveguide theory, and incorporating the effects of multipath propagation, noise interference, and metallic shielding in the downhole environment, a downhole electromagnetic wave transmission attenuation model is established. In this model, the transmitted signal propagates along the waveguide in a specific propagation mode while experiencing inherent losses caused by the waveguide walls and the surrounding medium. During propagation, the signal produces multipath components when encountering structural discontinuities, and each component exhibits different attenuation and propagation delay characteristics. When the signal passes through a metal barrier, such as during transmission from inside the drill pipe to the surrounding formation, significant attenuation occurs according to the metal shielding attenuation model.Ultimately, the severely attenuated signal is superimposed with strong downhole background noise and impulsive noise before reaching the receiver.

$$H_{total}(f,t) = H_{waveguide}(f) \cdot H_{multipath}(f,t) \cdot \exp[-a_{shield}(f) \cdot l] + N(f,t) \tag{10}$$

Where: $H_{waveguide}(f)$ is the frequency-domain transfer function derived from circular waveguide theory, which determines the attenuation and phase of the dominant propagation mode; $H_{multipath}(f)$ is the frequency response of the time-varying multipath channel generated by the multipath model; $exp[-a_{shield}(f) \cdot l$ is the additional shielding attenuation factor corresponding to the cumulative metal thickness penetrated; and N(f,t) is the frequency-domain

representation of the additive noise.

2.2. DPSK + FEC Modulation and Demodulation Signal Model

The transmitted electromagnetic wave signal is modulated using a combination of DPSK (Differential Phase Shift Keying) and FEC (Forward Error Correction). The original baseband data are encoded according to the FEC coding rules by inserting additional redundant parity bits into the original bit sequence, generating a coded bitstream containing information that is then fed into DPSK modulation. The input binary bitstream is treated as an absolute code and is converted into a relative code sequence representing phase changes through a differential encoder, thereby generating the final DPSK signal. The specific modulation and demodulation processes are illustrated in Fig 1.

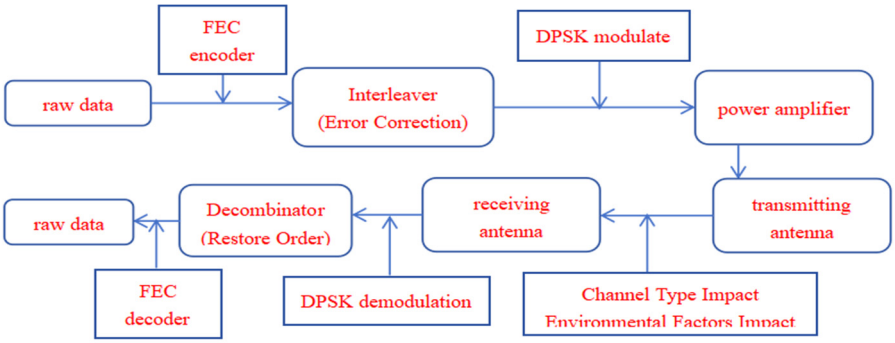

Fig 1. Signal flow diagram of DPSK + FEC modulation and demodulation

Data encoding and decoding are performed using convolutional codes and the Viterbi algorithm. In this study, a convolutional code with a constraint length of 7 (constraint length = shift register order + 1, namely a six-stage shift register $D^0 \sim D^6$)is adopted. The generator polynomials are $G_1 = 171$ (octal) and $G_2 = 133$ (octal). In the encoder structure (constraint length K=7), the input data pass through a six-stage shift register($D^0 \sim D^6$), generating two output bits c_1 and c_2:

$$\begin{cases} c_1 = d_i \oplus d_{i-1} \oplus d_{i-2} \oplus d_{i-3} \oplus d_{i-6} \\ c_2 = d_i \oplus d_{i-2} \oplus d_{i-3} \oplus d_{i-5} \oplus d_{i-6} \end{cases} \quad (11)$$

The first output c_1 corresponds to G_1=171 (octal) (binary: 1111001), where '1' corresponds to taps at D^6, D^4, D^3, D^1 and D^0. The second output c_2 corresponds to G_2=133(octal) (binary: 1011011), where '1' corresponds to taps at D^6, D^4, D^3, D^1 and D^0. The state of the convolutional code is defined by the contents of the shift register. When the constraint length K=7, the number of states is 2^{K-1}=64(a 6-bit register). The state representation is given as $S=(d_{i-1},d_{i-2},...,d_{i-6})$, resulting in a total of 64 possible combinations (ranging from 000000 to 111111). According to the state transition rule, each state transitions to a new state based on the input bit (0 or 1) and produces the corresponding output. The state transition relationships are shown in Table 1.

Table 1. Schematic diagram of transfer rule status

Current state($d_{i-1},d_{i-2},...,d_{i-6}$)	Input d_i	New state ($d_i,...,d_{i-5}$)	Outputc_1c_2
000000	0	000000	00
000000	1	100000	11
100000	0	010000	10
100000	1	110000	01
...	...	...	...

The encoded bitstream $b_n \in \{0,1\}$ is input into the differential encoding hardware modulator and converted into a relative code $d_n \in \{0,1\}$ through differential encoding. The phase variation of the relative code is expressed as shown in Equation (12).

$$\begin{aligned} d_n &= d_{n-1} \oplus b_n \\ \Delta\varnothing_n &= \begin{cases} 0, & d_n = 0 \\ \pi, & d_n = 1 \end{cases} \\ \varnothing_n &= \varnothing_{n-1} + \Delta\varnothing_n \end{aligned} \quad (12)$$

Its time-domain expression is given as follows:

$$s(t) = A\cos(2\pi f_c t + \varnothing_n), \quad (n-1)T \le t \le nT \quad (13)$$

Where: A represents the signal amplitude (V); f_c represents the carrier frequency (Hz); T represents the symbol period (s); and $\emptyset_n$ represents the phase of the n-th symbol (dimensionless).

Different signal waveforms can be obtained by setting different carrier frequencies. As the carrier frequency increases, the symbol period decreases, resulting in a denser signal waveform in the time domain and an increased number of transmitted symbols per unit time, which theoretically improves the data transmission rate, as shown in Equation (14).

$$T_s = \frac{1}{R_s} \le \frac{1}{B} \propto \frac{1}{f_c} \quad (14)$$

After the electromagnetic wave signal is received, it is fed into the DPSK demodulator at the receiver. DPSK recovers the relative code by comparing the phase difference between adjacent symbols, and the bitstream containing redundant information is then obtained through inverse differential decoding. After low-pass filtering, the bitstream is sent to the FEC decoder, where the matching degree between the received sequence and all possible encoded sequences is calculated. The optimal path is selected and traced back for error correction, ultimately producing the error-free original bitstream. The demodulation principle is as follows: the current received symbol $s_n(t)$ is multiplied by the signal $s_{n-1}(t-T)$ delayed by one symbol period T from the previous symbol to extract the phase difference information.

$$r(t) = s_n(t) \cdot s_{n-1}(t-T) = \frac{A^2}{2}\left[\cos(4\pi f_c - 2\pi f_c T + \varnothing_n + \varnothing_{n-1}) + \cos(2\pi f_c T + \varnothing_n - \varnothing_{n-1})\right] \quad (15)$$

"Where: the high-frequency component is $\cos(4\pi f_c - 2\pi f_c T + \emptyset_n + \emptyset_{n-1})$, with a frequency of $2f_c$, which does not carry phase difference information and must be completely removed by subsequent low-pass filtering. The low-frequency component is $\cos(2\pi f_c T + \emptyset_n - \emptyset_{n-1})$, which carries the phase difference information $\Delta\emptyset_n$ and serves as the key factor for subsequent decision-making. The frequency response H(f) allows only the baseband frequency to pass while suppressing the high-frequency components. The corresponding time-domain impulse response h(t) is given as follows:

$$h(t) = \frac{\sin(\pi t / T_s)}{\pi t / T_s} \cdot \frac{\cos(\pi \alpha t / T_s)}{1 - (\pi \alpha t / T_s)^2} \quad (16)$$

Where: T_s is the symbol period (s); and α is the roll-off factor (dimensionless).

Finally, the low-frequency component is obtained as follows:

$$r_{LPF}(t) = \frac{A^2}{2}\cos(2\pi f_c T + \Delta\varnothing_n) \quad (17)$$

In practical communication systems, the integer-cycle condition is usually satisfied, where the symbol period T is an integer multiple of the carrier period $T_C = 1/f_c$ (that is, $T = kT_C$). Under this condition, the following relationship holds:

$$2\pi f_c T = 2\pi f_c \cdot \frac{k}{f_c} = 2\pi k \quad (18)$$

$$r_{LPF}(t) = \frac{A^2}{2}\cos(\Delta\varnothing_n) \quad (19)$$

Under this condition, the decision variable depends only on the phase difference $\Delta\emptyset_n$ and is independent of the carrier frequency f_c, thereby eliminating its interference with the decision process. Based on the filtered signal $r_{LPF}(t)$, the decision is made as follows: if the polarity of the product signal is positive, it is determined as '0'; if the polarity of the product signal is negative, it is determined as '1', as expressed in the following equation:

If the polarity $r_{LPF}(t)$ is positive, that is, $\cos(\Delta\emptyset_n) > 0$, it corresponds to $\Delta\emptyset_n = 0$

If the polarity $r_{LPF}(t)$ *is negative*, that is, $\cos(\Delta\emptyset_n) < 0$, it corresponds to $\Delta\emptyset_n = \pi$

$$\begin{aligned} PM_t(s) &= \min_{s' \in prev(s)}[PM_{t-1}(s') + d_t(s' \to s)] \\ SP_t(s) &= \arg\min_{s' \in prev(s)}[PM_{t-1}(s') + d_t(s' \to s)] \\ \hat{\mu}_t &= bit(SP_{t+1}(s_{t+1}) \to s_t) \end{aligned} \quad (20)$$

Where: $PM_t(s)$ is the path metric; prev(s) is the set of previous states that can transition to the current state s; the initial condition is $PM_0(s_0)=0$; $d_t(s)$ is the Hamming distance at the current time; $SP_t(s)$ is the survivor path; μ_t is the decoded output at time t (that is, the recovered original downhole baseband information); and bit(·) is the function that maps the state transition back to the input bit.

3. Design and Performance Testing of the Wireless Transmission Device

3.1. Design of a Wireless Transmission System Based on DPSK and FEC

Faced with the high-temperature and high-pressure downhole environment, the DPSK + FEC scheme replaces complex analog hardware with algorithmic redundancy, eliminating the need for carrier recovery circuits; only a delay multiplier and a low-pass filter are required to perform phase difference detection. FEC adds redundant parity bits at the transmitter, allowing the receiver to automatically correct bit errors, thereby reducing the accuracy requirements for front-end RF and analog hardware. In addition, FEC can tolerate a certain level of quantization error. Therefore, an ADC/DAC with improved temperature resistance and moderate precision is designed to reduce heat dissipation paths and lower power consumption. The downhole electromagnetic wireless transmission acquisition board is powered by a lithium battery with a rated output of 3.3 V, meeting the MCU's operating voltage requirements. After a boost circuit, the voltage is increased to 5 V to meet the operating voltage requirements of downstream devices such as temperature sensors, pressure sensors, and antennas. The hardware system is shown in Fig 2.

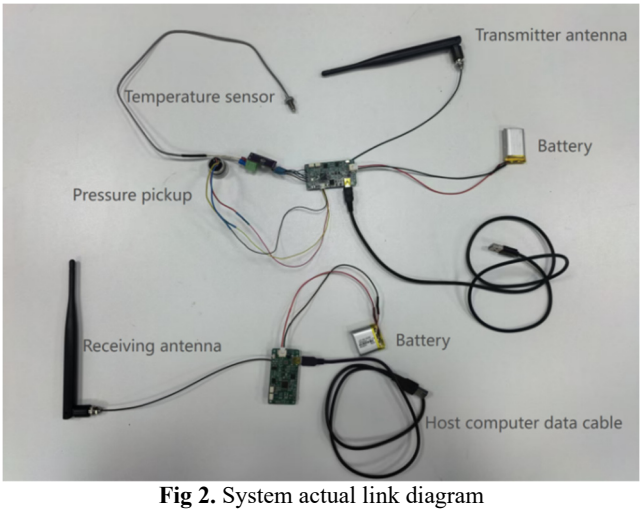

Fig 2. System actual link diagram

3.2. Performance Test Results

In a temperature- and humidity-controlled indoor environment, the downhole electromagnetic wireless transmission system was tested to verify its functional reliability. A comprehensive analysis and verification were conducted from the perspectives of metal shielding and penetration through different media. The effects of various factors on electromagnetic wave transmission were evaluated to determine the optimal propagation conditions and metal shielding resistance performance. The experimental setup is shown in Fig 3.

(a) Transmission Test in Metal Sheath

(b) Metal box shielding effect

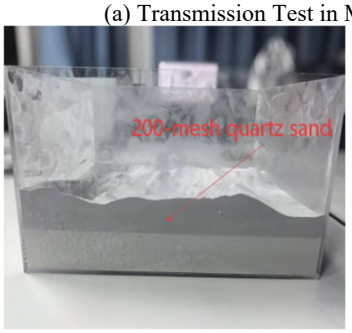

(c)sand transport exp

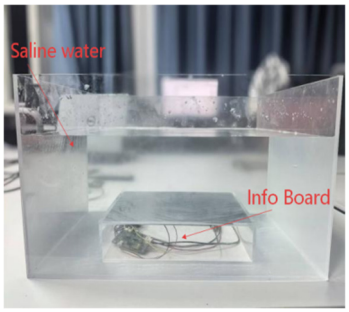

(d)salt water transport exp

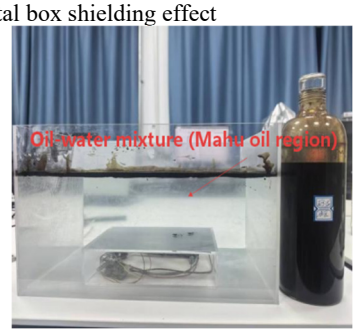

(e)oil-water transfer exp

Fig 3. Signal transmission experiment

The test results show that the system maintains a stable transmission efficiency above 90% with fluctuations less than 5% in low-attenuation media such as sand or oil-water mixtures. This verifies that the differential coding mechanism of DPSK can effectively suppress phase drift caused by multipath interference, while FEC compensates for bit errors resulting from medium attenuation and distortion. Even in high-attenuation media such as water, the transmission efficiency remains above 85%, significantly outperforming schemes without FEC, demonstrating the strong error-correcting capability of FEC.

Under metal-shielded conditions, the system also demonstrates strong adaptability. In carbon steel casings (partial shielding), the transmission efficiency remains 71.94% at a 3-meter separation, indicating that DPSK can tolerate phase drift and attenuation caused by metal, while FEC further corrects the associated bit errors. In a partially open metal box (weak shielding), the system maintains 6.94% efficiency with a 10° opening and only experiences interruption when fully enclosed, demonstrating its ability to sustain communication even under extreme shielding conditions.

Table 2. Analysis of Signal Transmission Influenced by Transmission Medium

Transmission results in soil medium	Test group	System efficiency
	1	94.72%
	2	91.67%
	3	96.12%
	4	92.22%
	5	89.72%
	6	94.17%
Transmission results in water medium	Test group	System efficiency
	1	92.50%
	2	90.83%
	3	87.78%
	4	84.72%
	5	90.00%
	6	86.11%
Transmission results in oil–water mixture	Test group	System efficiency
	1	93.35%
	2	91.82%
	3	92.33%
	4	90.46%
	5	88.57%
	6	85.67%

Table 3. Metal shielding effect test

3.1m 7.32mm Transmission data through carbon steel casing						
Distance/m	1	1.5	2	2.5	3	
System efficiency	86.39%	83.33%	81.39%	76.67%	71.94%	
205*150*100mm Transmission data through metal box						
Opening size/°	180	60	40	20	10	0
System efficiency	97.50%	46.94%	43.33%	24.44%	6.94%	0%

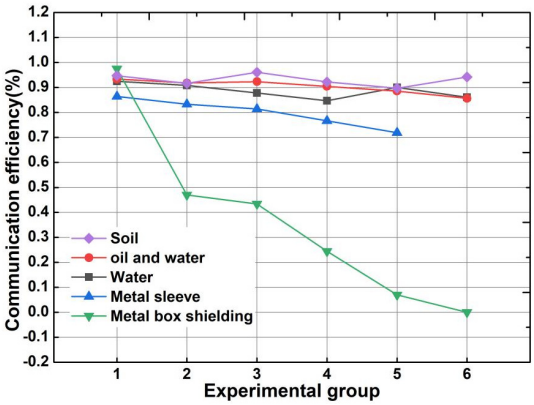

Fig 4. Influence factor error rate curve

The experiments validated that the designed transmission signal exhibits good penetration through various media. In addition, the data on medium attenuation and metal shielding obtained from the experiments were programmed into the transmission hardware. By dynamically adjusting parameters such as the DPSK + FEC coding rate and transmit power, a balance between transmission efficiency and reliability can be achieved, enabling the simulation of long-distance, multi-medium transmission characteristics.

4. Simulation of Downhole Industrial Signal Transmission

The system's transmitted electromagnetic wave signals were experimentally simulated under actual downhole operating conditions to observe the effects of factors such as downhole noise interference, formation media variations, temperature, and transmission distance on signal attenuation, waveform distortion, and bit error rate. These tests validated the adaptability and anti-interference capability of the DPSK + FEC combined modulation technique in complex downhole environments.

4.1. Simulation Testing of Downhole Noise Environment Interference

After generating the baseband and DPSK signals in MATLAB, the signals were transmitted through a Gaussian white noise channel to simulate the downhole noise environment (Fig 5). The received signals were processed through low-pass filtering, sampling and decision-making, differential decoding, and FEC error correction to verify the recovery of the baseband information.

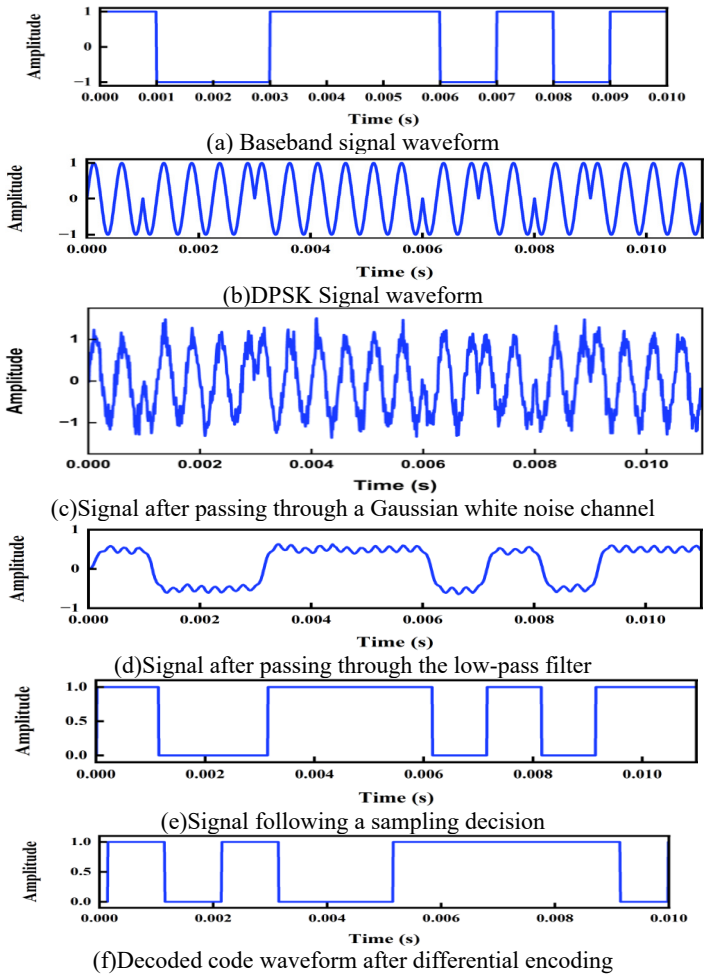

(a) Baseband signal waveform

(b)DPSK Signal waveform

(c)Signal after passing through a Gaussian white noise channel

(d)Signal after passing through the low-pass filter

(e)Signal following a sampling decision

(f)Decoded code waveform after differential encoding

Fig 5. Noise simulation in mine

The noise energy of Gaussian white noise is uniformly distributed across the entire frequency band, and its instantaneous amplitude follows a zero-mean normal distribution, which is highly consistent with the broadband random interference characteristics caused by downhole multipath reflections and electromechanical equipment noise[21]. Its power spectral density and probability density function are given in Equation (21). The absence of a fixed bias aligns with the practical downhole electromagnetic interference scenario, which exhibits no directional trend.

$$S_n(f)=\frac{N_0}{2},\quad (f\in[-\infty,+\infty])$$
$$f_n(x)=\frac{1}{\sqrt{2\pi\sigma_n^2}}\exp\left(\frac{-x^2}{2\sigma_n^2}\right) \tag{21}$$

Where: N_0 is the single-sided power spectral density of the noise (W/Hz); x is the instantaneous value of the noise (V); $\sigma^2{}_n$ is the noise variance (dimensionless) with a mean $E[n(t)]=0$.

From the simulation waveforms, it can be clearly observed that the original baseband signal, after DPSK modulation, forms a phase-encoded carrier signal. After transmission through the Gaussian white noise channel, the signal exhibits noticeable amplitude fluctuations and superimposed noise, and a few bit errors remain after sampling and decision-making. However, after FEC decoding and error correction, the final output waveform matches the original baseband signal level sequence perfectly, with no noticeable distortion or missing bits. This result demonstrates that FEC, by introducing redundant parity bits at the transmitter, can accurately detect and actively correct random bit errors caused by noise. Meanwhile, the noncoherent demodulation mechanism of DPSK eliminates the need for carrier synchronization and effectively avoids the impact of noise-induced phase drift on demodulation. The combination of the two thus achieves dual interference resistance against downhole noise.

4.2. Simulation of Electromagnetic Wave Transmission under Actual Downhole Conditions

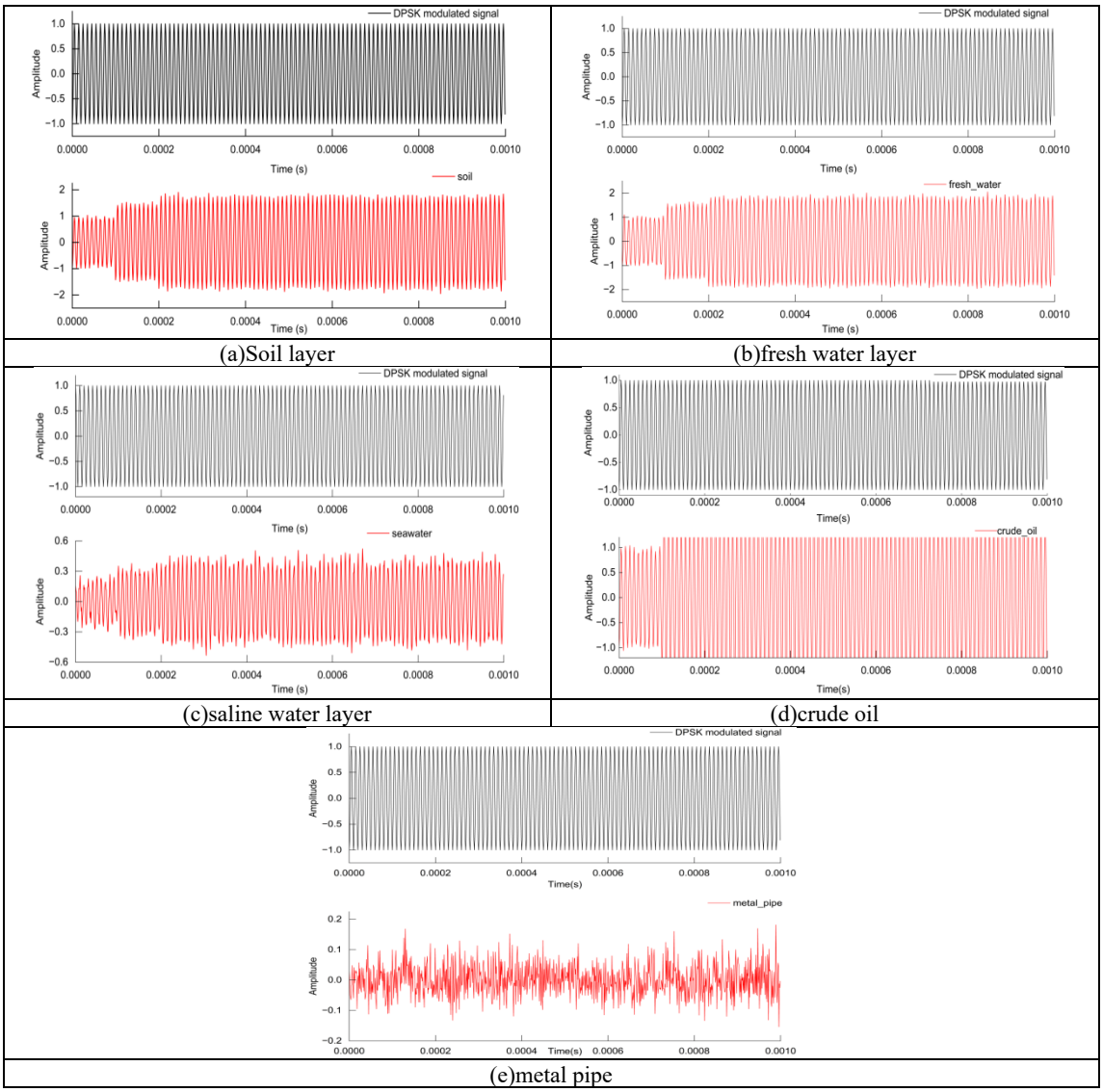

(a)Soil layer (b)fresh water layer

(c)saline water layer (d)crude oil

(e)metal pipe

Fig 6. Effects of different media on transmission signal

The base signal modulated with DPSK + FEC was generated in MATLAB. With fixed parameters such as carrier frequency, transmit power, and ambient temperature, transmission simulations were conducted through five typical

downhole media—soil, fresh water, saline water, crude oil, and metal pipes—to evaluate performance across four dimensions: signal attenuation, waveform distortion, bit error rate, and communication quality (Fig 6, Table 4). Additionally, the effects of temperature gradients and increased well depth on signal transmission were simulated to clarify the influence of environmental parameter variations (Fig 8 and 9). Finally, multiple temperature–distance combinations were tested to verify the system's stable operational range under complex compound downhole conditions (Fig 10).

Fig 6 shows the time-domain waveform variations of the DPSK + FEC modulated signal in five different media. Combined with the quantitative analysis in Table 4, the conductivity and permittivity of the media are identified as the key factors determining signal transmission performance. The transmission performance decreases in a stepwise manner with increasing medium conductivity, and the transmission characteristics of the different media exhibit a distinct layered pattern.

Table 4. Transmission effects and performance differences of five media

Medium type	Degree of signal attenuation	Degree of waveform distortion	Expected bit error rate (BER)	Transmission performance
crude_oil	Very weak	Very light	$\approx 10^{-5}$	Best
soil	Modearte	Moderate	$\approx 10^{-4}$	Better
fresh_water	Moderate	Moderate	$\approx 10^{-3}$	Normal
seawater	Relatively strong	Relatively heavy	$\approx 10^{-2}$	Relatively poor
metal_pipe	Very strong	Very heavy	≈0.5	Worst

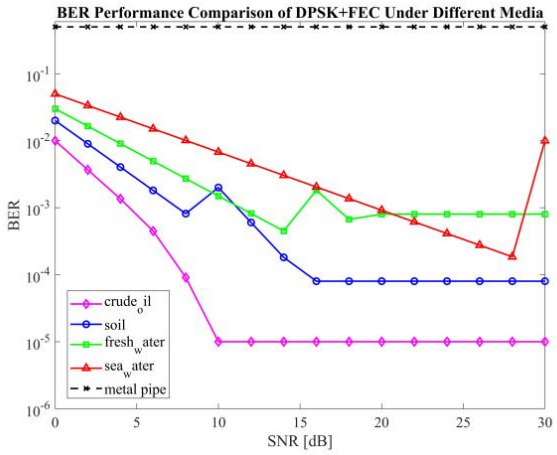

Fig 7. Comparison of five media bit error rate

As shown in the BER–SNR curves in Fig 7, it can be further verified that under the same SNR conditions, the BER in crude oil and soil media is significantly lower than that in fresh water and saline water, and the BER decreases more rapidly as the SNR increases. In contrast, the BER in the metal pipe remains approximately 0.5 and shows little variation with changes in SNR.These results indicate that the interference-resistance advantage of the DPSK–FEC combined modulation scheme can be effectively realized only in low- to medium-attenuation media. In high-attenuation media, system performance is mainly constrained by the electromagnetic properties of the medium itself, and only limited improvement can be achieved by further increasing the SNR. In metallic environments such as metal pipes, the proposed technique becomes ineffective due to strong reflections and eddy current losses occurring at the metal surface.

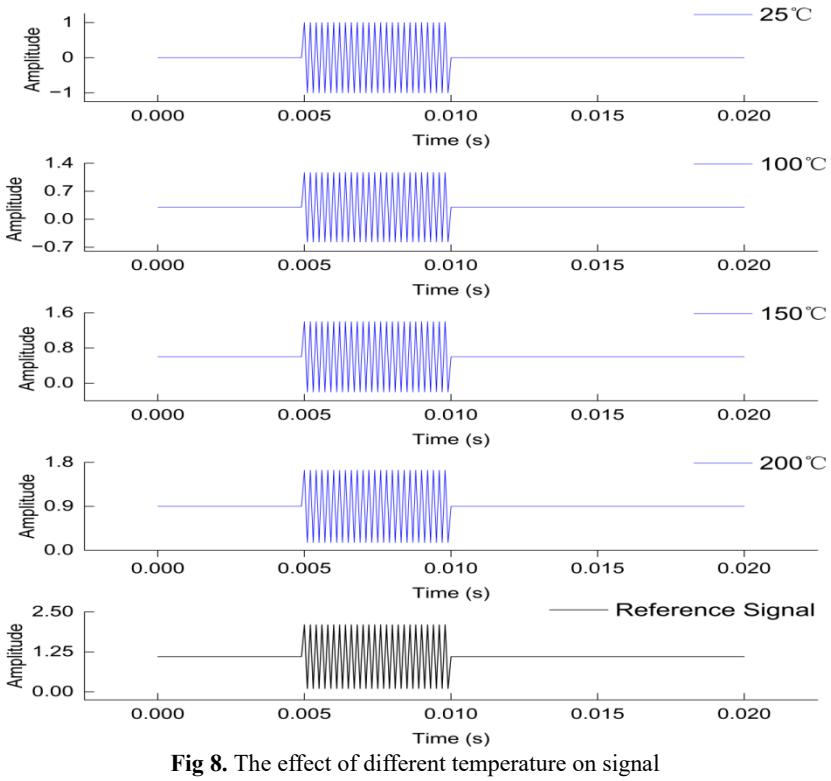

Fig 8. The effect of different temperature on signal

Fig 8 shows the received waveforms and amplitude variations of the DPSK + FEC modulated signal at different

temperatures. Downhole temperature increases with well depth, and temperature changes directly alter the permittivity and conductivity of the formation media. For every 50 °C increase in temperature, the medium's conductivity rises by approximately 1–2 orders of magnitude, resulting in greater amplitude attenuation, increased phase drift, and more severe waveform distortion[22]. The calculations indicate that at 25 °C (room temperature), the received signal amplitude is stable with no significant phase shift. When the temperature rises to 75 °C, the signal amplitude attenuates by approximately 20%, with minor fluctuations. At 125 °C, the signal amplitude attenuates by over 50%, phase drift becomes significant, and noticeable intersymbol interference appears. Additionally, increasing temperature transforms the downhole channel from a static to a time-varying channel; dynamic changes in the electromagnetic properties of the medium enhance the randomness of multipath effects, further increasing the bit error rate and adding complexity to demodulation and error correction. Nevertheless, even at 125 °C, effective baseband signals can still be recovered through DPSK demodulation and FEC correction. These results demonstrate that the proposed method is adaptable to high-temperature downhole gradients and can maintain effective communication at temperatures below 125 °C.

Fig 9 presents the characteristic curve of signal attenuation with increasing well depth. The attenuation of downhole low-frequency electromagnetic signals rises exponentially with transmission distance. The additional shielding loss from metal casings causes the overall signal attenuation rate to be much higher than the attenuation caused by depth alone. Without metal casings, the signal amplitude attenuates by approximately 10 dB at 500 m, 25 dB at 1000 m, and 40 dB at 1500 m. In the presence of metal casings, the signal attenuation at the same depth increases by an additional 10–15 dB, and at 3000 m depth, the signal amplitude has decayed to the noise floor and is no longer detectable. The exponential signal decay with depth directly reduces the signal-to-noise ratio and causes the bit error rate to rise exponentially, significantly compressing the system's effective communication range. To compensate for the attenuation due to depth and casing, measures such as increasing transmit power, improving receiver sensitivity, and optimizing coding rates are required to enhance the system's anti-attenuation capability.

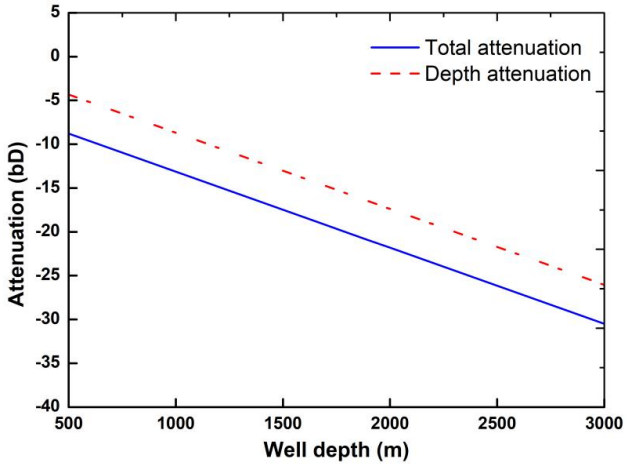

Fig 9. depth-dependent attenuation characteristics

Nine combined scenarios were set up with three temperatures (25 °C, 75 °C, 125 °C) and three transmission distances (500 m, 1000 m, 1500 m) to simulate the synergistic effects of downhole temperature and distance. The comprehensive performance of the DPSK + FEC combined modulation technique was evaluated, and the results are shown in Fig 10. The calculation results indicate that the system's bit error rate (BER) increases significantly with rising temperature and transmission distance, with distance having a much greater impact on BER than temperature. The DPSK + FEC modulated signal demonstrates stable and reliable performance across multiple environments. The curves of different colors, representing different depths and temperatures, converge in the high SNR region, with the BER approaching a very low level. Despite downhole environmental variations—such as increased attenuation due to greater depth and changes in the medium's electromagnetic properties caused by temperature fluctuations—the DPSK + FEC modulation can still reduce the BER to very low levels, demonstrating strong adaptability to complex downhole conditions characterized by high attenuation and variable temperature. The system can actively detect and correct transmission errors, maintaining a low BER even at relatively low SNR, thereby providing significant "error-correction gain"and reducing stringent requirements on transmit power or receiver sensitivity. In Fig 10, data transmission remains effective at a transmission distance of 1000 m and an ambient temperature of 125 ℃.

5. Conclusion

This study addresses key challenges in downhole electromagnetic wireless transmission, such as high attenuation, multipath interference, low signal-to-noise ratio, and dynamic variations in environmental parameters, by proposing a combined modulation method based on Differential Phase Shift Keying (DPSK) and Forward Error Correction (FEC). A downhole channel model incorporating path loss, multipath effects, noise interference, and metal shielding was established, and a corresponding hardware system was designed. Multi-dimensional simulation experiments were conducted to evaluate the transmission characteristics, performance metrics, and applicable range of the system under realistic downhole conditions. The main conclusions are as follows:

(1) The DPSK + FEC downhole low-frequency electromagnetic wireless transmission system can achieve stable operation at transmission distances up to 1000 m and ambient temperatures up to 125 °C. When the received SNR is ≥15 dB, the system's bit error rate (BER) can be stably reduced to below the required level, meeting the real-time transmission requirements for critical downhole parameters such as temperature, pressure, and position. Under conventional downhole conditions with transmission distances ≤500 m and temperatures ≤75 °C, a received SNR ≥10 dB is sufficient to achieve high-reliability transmission with BER below the target threshold.

(2) The system performance optimization focuses on four dimensions: transmitter parameters, coding strategy, hardware configuration, and signal preprocessing, with each optimization measure having clearly defined adjustment values and quantified performance improvements. For medium- to high-attenuation media (e.g., saline layers or highly mineralized water layers with conductivity of 50–100 S/m), increasing the transmit power results in a synchronous increase in received SNR; specifically, for every 5 dB increase in transmit power, the receiver SNR rises by

5 dB and the system BER decreases by one order of magnitude. For example, in a saline layer, increasing the transmit power from 10 dBm to 20 dBm reduces the BER from [value] to [value]. To reduce the FEC coding rate, the convolutional code rate was adjusted from 1/2 to 1/3, enhancing error-correction capability by 40%, which compensates for 10–15 dB signal loss due to medium attenuation and improves transmission efficiency by 10–15%.

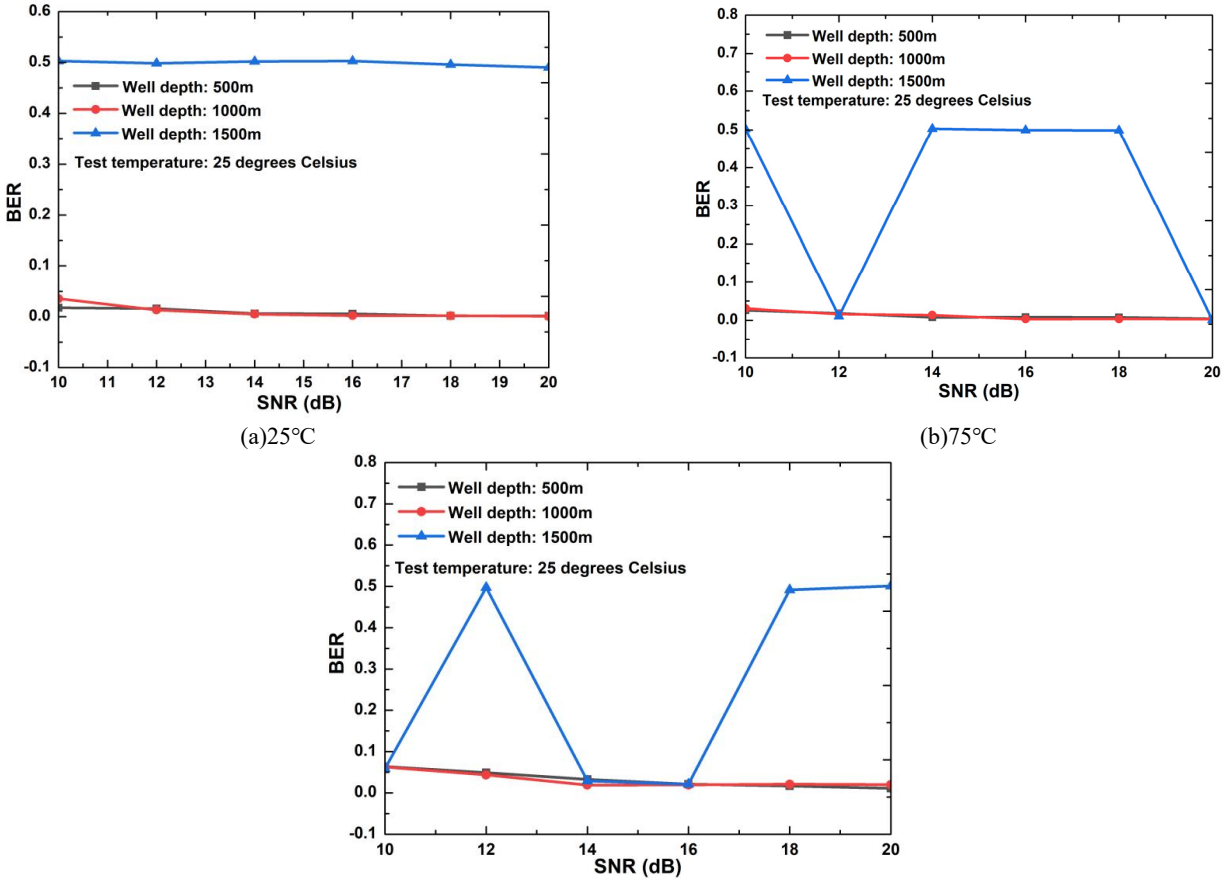

(a)25℃ (b)75℃

(c)125℃

Fig 10. Performance curve of signal bit error rate in different environments

(3) For high-temperature downhole conditions (75 °C–125 °C), lowering the DPSK carrier frequency can compensate for phase distortion caused by elevated temperatures, resulting in a 50% reduction in BER at the same temperature. When using ADC/DAC chips rated for 150 °C, compared to 75 °C-rated chips, hardware quantization errors under high temperature are reduced by 60%, and signal waveform distortion decreases by 40%. For metal-shielded or deep-well conditions (including carbon steel casings / well depths of 1000–1500 m), increasing the antenna gain from 2 dBi to 5 dBi triples the received signal amplitude, compensating for the additional 10–15 dB attenuation caused by the casing. Optimizing the receiver sensitivity from −100 dBm to −110 dBm allows detection of weaker attenuated signals, extending the effective communication distance from 1000 m to 1500 m while maintaining BER below the target threshold. For high-noise wells (strong downhole electromechanical interference, SNR < 10 dB), adding a digital filtering stage can suppress over 90% of high-frequency electromagnetic interference, improving the received SNR by 6–8 dB. By optimizing the FEC interleaving depth, increasing it from 256 to 512, the system's resistance to pulse noise improves by 50%, reducing BER from 10^{-2} to below 10^{-3}. For wells with significant multipath effects (irregular wellbore/strong formation reflections), adjusting the DPSK symbol period from $1\mu s$ to $2\mu s$ enhances inter-symbol interference suppression by 40%. Combined with multipath mitigation algorithms, BER caused by multipath propagation can be reduced by 60%.

Acknowledgments

This research is supported by National Major Science and Technology Project of China "Phase-Mixed Drive Technology and Integrated Demonstration for CCUS-EOR in Conglomerate Reservoirs of the Junggar Basin" (grant no. 2025ZD1408405).

References

[1] Craig J, Hakhoo N, Bhat G M, et al. Petroleum systems and hydrocarbon potential of the North-West Himalaya of India and Pakistan[J]. Earth-science reviews, 2018, 187: 109-185.

[2] Kisseleff S, Akyildiz I F, Gerstacker W H. Digital signal transmission in magnetic induction based wireless underground sensor networks[J]. IEEE Transactions on Communications, 2015, 63(6): 2300-2311.

[3] Yu Y, Huang S, Wang J, et al. Design of wireless logging instrument system for monitoring oil drilling platform[J]. IEEE Sensors Journal,2015,15(6):3453-3458.

[4] Zhang L, Yang W, Fang W, et al. Periodic Monitoring and Filtering Suppression of Signal Interference in Mine 5G Communication[J]. Applied Sciences, 2022, 12(15): 7689.

[5] Liu Y. Analysis on present status and development trend of shale gas ground engineering technology [J]. Chemical Engineering of Oil & Gas, 2019, 48(3): 66-71.

[6] Dong R, Fujita Y, Nakamura H, et al. Electromagnetic penetration and reflection analysis in fractal structures using three-dimensional empirical mode decomposition[J]. IEEE Transactions on Magnetics, 2022, 58(9): 1-4.

[7] Pan Z. Study on In-Pipe Electromagnetic Signal Wireless Transmission System Based on Spread Spectrum Technology [D]. Xi'an Shiyou University, 2024. DOI:10. 27400/ d. cnki. gxasc. 2024.001166.

[8] Ghaddar M, Mabrouk I B, Nedil M, et al. Deterministic modeling of 5G millimeter-wave communication in an underground mine tunnel[J]. IEEE Access, 2019, 7: 116519-116528.

[9] Zi G, Ma Z, Wang Y, et al. Miniaturized Low-Frequency Communication System Based on the Magnetoelectric Effect[J]. Micromachines, 2023, 14(10): 1830.

[10] Goldsmith A J, Chua S G. Adaptive coded modulation for fading channels[J]. IEEE Transactions on communications, 1998, 46(5): 595-602.

[11] Dai J, Chen X, Zhang F, et al. Optimisation design of systematic fountain codes on fading channels[J]. IET Communications, 2019, 13(20): 3369-3376.

[12] Zhou H, Xiao P, Woo W L, et al. Expanded decorrelating detector with reduced noise enhancement for multipath frequency-selective fading channels[J]. IET communications, 2008, 2(1): 164-173.

[13] Li F, Chen J ,Wu J , et al. Research on High Speed Communication Method of ELF-EM While Drilling Based on Adaptive Combined Filtering Algorithm [J]. China Communications, 2023, 20 (06): 129-147.

[14] Savchenko Y, Liu Y. Optimizing degree distributions of LT-based codes with deep reinforcement learning[C]//IEEE INFOCOM 2019-IEEE Conference on Computer Communications Workshops (INFOCOM WKSHPS). IEEE, 2019: 228-233.

[15] Afuekwe A, Bello K. Use of smart controls in intelligent well completion to optimize oil & gas recovery[J]. J. Eng. Res. Rep, 2019, 5: 1-14.

[16] Wang S, Liu X. Design and Implementation of DPSK Signal Modulation and Demodulation Based on FPGA [J]. Electronic Test, 2019, (09): 82-83+75. DOI:10.16520/j.cnki.1000-8519. 2019. 09.033.

[17] Han W K, Kumar L S, Guan Y L, et al. Design of coded digital telemetry system for acoustic downhole channel with drilling noise[C]//2013 9th International Conference on Information, Communications & Signal Processing. IEEE, 2013: 1-5.

[18] Xinshu Wu. Research on Communication Systems Based on Wireless Power Transfer Technology [D]. Yangzhou University, 2021. DOI: 10.27441/d.cnki.gyzdu.2021.001396.

[19] Lin J C. Study of MR-DPSK modulation[J]. IEEE communications letters, 2002, 6(4): 132-134.

[20] Chen L. The Design of the DPSK Signal Circuit and System Simulation [J]. Modern Industrial Economy and Informationization, 2017, 7 (16): 21-23. DOI:10.16525/j. cnki.14-1362/n.2017.16.08.

[21] Hu C, Zhang M, Zhang Q, et al. RESEARCH ON WIRELESS TELEMETRY TECHNOLOGY OF DOWHHOLE TEST DATA [J]. Drilling & Production Technology, 2011, 34 (01): 48-51+115-116.

[22] Li S, Yang Z, Luo L, et al. Analysis of Temerature Rise Effects of Magnetic Field in Paraxial Solenoids for Azimuth Transmission Systems [J]. Acta Optica Sinica, 2025, 45 (22): 258-269.